Dead time duration and active reset influence on the afterpulse probability of InGaAs/InP SPAD based SPDs

July 6, 2021

A. V. Losev 1,2,3 , A. A. Koziy 1,3 , V. V. Zavodilenko 1,3 , K. I. Khomyakova 4 , Y. V. Kurochkin 1,3 , A. A. Gorbatsevich 2,5

¹"Qrate" LLC, St. Novaya, d. 100, Moscow region, Odintsovo, Skolkovo village, 143026, Russia.
²National Research University of Electronic Technology MIET, Shokin Square, 1, Zelenograd, 124498, Russia.

³NTI Center for Quantum Communications, National University of Science and Technology MISiS, Leninsky prospekt 4, Moscow, 119049, Russia

⁴National Research Tomsk State University, Lenin Av. 36, Tomsk, 634050, Russia ⁵P.N. Lebedev Physical Institute of the Russian Academy of Sciences, Leninsky prospect, 53, Moscow, 119333, Russia.

Abstract

We have performed a detailed study of the dependence of afterpulse probability in InGaAs/InP sine-gated SPAD on the dead time and the existing approach for its implementation. We have found that the comparator's simple latching can significantly reduce the probability of afterpulse, even without using a dead time pulse that lowers the diode bias voltage. We have established that with low probability of afterpulse (< 5 %) or with large dead time ($\tau > 10~\mu s$), it is sufficient to use a circuit with latching of the comparator, which will significantly simplify the development of an SPD device for applications in which such parameters are acceptable. We have also proposed a precise method for measuring the afterpulse and presented a model describing the recurrent nature of this effect. We have demonstrated that a simple model should not be used for afterpulse probability measurement due to rough underlying physical processes. A second-order model is preferable.

1 Introduction

Detectors based on superconducting nanowires (SNSPD) [1] and single photon avalanche diodes (SPAD) [2] have proven themselves in the best way as single-photon detectors (SPDs). Each of the implementations has both its advantages and disadvantages. SNSPD has high probability of photon detection and low noise level, but it is large and quite expensive due to usage of helium cryostat [3]. SPAD-based SPDs have small size and low cost, but detection probability is relatively low, and noise characteristics are high. In QKD, both first and second types of SPD have found their application [4,5]. It is advisable to use SNSPD for key distribution over long distances, both over fiber and open space. SNSPD based QKD was able to demonstrate key distribution distance records [6]. It is advisable to use SPAD-based SPD in small-sized industrial installations [7] that distribute the key within one city or even one building since the loss of photons in the line is minimal and the key generation rate is relatively high.

One of the big problems of the QKD is the difficulty of determining the secrecy of the generated key. In contrast to classical cryptographic algorithms, in which applied mathematical transformations strictly determine confidentiality of the key, quantum cryptography depends on the installation's physical parameters [8]. Thus, calculated key secrecy can be selected pessimistically, which will significantly reduce key generation rate or optimistically, which will endanger security of subsequently encrypted data. For this reason, development of methods for accurate determination of the parameters of SPD is an actual task that can significantly increase the efficiency of the QKD installation as a whole [9].

In SNSPD with adequate control electronics, there are no effects associated with previous triggers [10]. Therefore, we can consider all processes as Markovian [11]. There is "memory" of earlier triggers in SPAD-based SPDs – the processes have more complicated influence on counting statistics [12], and the construction of a global SPD model becomes complicated. Charges captured by the traps cause this memory. These charges relax after particular time, which can be determined experimentally, and are called afterpulses [13].

For detectors of 1550 nm wavelength photons, based on InGaAs/InP SPAD, total relaxation time is about $1-50~\mu s$ at a temperature of about $-100-50~\rm C$. For Si-based photon detectors for visible radiation, full relaxation time is about 200 ns [14]. To overcome afterpulsing, the following methods are used: usage of SPD circuits with dead time – the time during which new triggering cannot be recorded by the detector after the previous triggering; lowering avalanche growing time by fast quenching. We can use high dead time, but SPDs used in QKD receive significant restrictions on the limiting operating frequencies, which harms the installation's efficiency as a whole. Therefore, to obtain the SPD's highest efficiency for the QKD application, the dead time value is reduced to $1-10~\mu s$ while sacrificing QBER but gaining maximum count rate, which is especially important for short distances QKD [15].

In this work we observe only the dead time approach for afterpulse control. We investi-

gated two possible technical realizations of the dead time: it includes comparator latching (passive quenching and reset) as well as active bias lowering (passive-active quenching and reset). We analyzed these two methods and made recommendations on using one of them in different practical cases. We made recommendations for setting time parameters of latching the comparator based on statistical data analysis and the physics of the processes. Also, the empirical models' parameters approximating the experimental data, which allows them to be used in subsequent global SPD models, were given.

We developed an accurate method for calculation of the detector's afterpulse probability from counting statistics. Several models of its calculation were proposed and then analyzed based on experimental data obtained from custom sinusoidal gated SPDs based on InGaAs/InP SPAD. However, the results obtained are also applicable to SPD based on other SPAD structures.

Different approaches to extraction of afterpulse probability from counting statistics were proposed [16–19]. However, there is no consensus on which experimental setup, settings and models should be using for obtaining afterpulse probability. In our work we compare afterpulse probability, obtained with widely used simple model [16] to afterpulse probability obtained with our own model. We recieved a result, confirming that afterpulse probability value sufficiently differs when it is obtained with the use of our model.

2 Simple and complex afterpulse models

Afterpulse probability is the probability that the next detector's trigger ("click") generated by the afterpulse mechanism will occur after any trigger [9]. According to this definition, the afterpulse click can trigger the next afterpulse click (second-order afterpulses). This effect is negligible for low afterpulse probabilities ($p_{ap} < 5\%$) but should be carefully accounted for high. In this section, we present two different models – "Simple" and "Complex". The advantage of the simple model is its simplicity and possibility of easy p_{ap} calculation from the statistics. The advantage of the complex model is that it is an accurate statistical description of afterpulse processes in the diode.

The simple model's main idea is the afterpulse click probability P_{ap}^s can be derived from photon-, thermal-, tunneling- induced click probabilities P_0 by the parameter p_{ap}^s .

$$P_{ap}^s = P_0 p_{ap}^s. (1)$$

In this view, the P_{ap}^s included the second, third, etc. order afterpulses, and its assessment is included in the parameter p_{ap}^s . This approach is right for the low afterpulse probabilities because the high-order afterpulses are unlikely. The main drawback is that with varying the P_0 by, for example, an increase in the number of photons per pulse, the p_{ap}^s assessment will differ too [15]. We can find the total probability of click P from the schematic diagram 1 a).

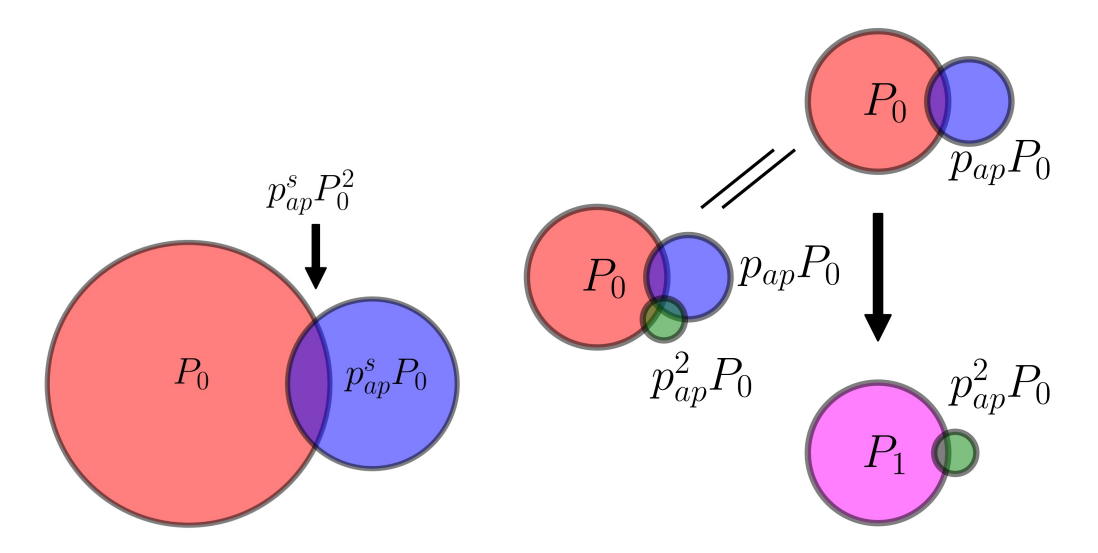


Figure 1: Schematic diagram of afterpulse probability models: a) simple model; b) complex model. P_0 is a probability of clicking in a system without afterpulse, p_{ap} – is the afterpulse probability.

The total click probability P can be derived as:

Simple:
$$P = P_0 + P_{ap}^s - P_0 P_{ap}^s = P_0 (1 + p_{ap}^s - P_0 p_{ap}^s)$$
 (2)

In the complex model, we take into account the recursive behavior of the afterpulse. In this case, we can show the next schematic diagram, presented in figure 1 b).

The probability that the clicks P_0 will generate an afterpulse is equal to P_0p_{ap} . The probability that afterpulses P_0p_{ap} generate new afterpulses is P_0p_{ap} , and so on. The calculation of the overall afterpulse influence on the total probability of click can be performed by a series of consecutive convolutions of probabilities $(P_1, P_2, \text{ etc.})$. We can write the next equations:

$$P_{1} = P_{0} + P_{0}p_{ap} - P_{0}P_{0}p_{ap} = P_{0}(1 - P_{0}p_{ap}) + P_{0}p_{ap},$$

$$P_{2} = P_{1} + P_{0}p_{ap}^{2} - P_{1}P_{0}p_{ap}^{2} = P_{1}(1 - P_{0}p_{ap}^{2}) + P_{0}p_{ap}^{2},$$

$$\vdots$$

$$P_{i+1} = \dots = P_{i}(1 - P_{0}p_{ap}^{i+1}) + P_{0}p_{ap}^{i+1}.$$

$$(3)$$

This recurrent equation can be rewritten as the decomposition relate parameter P_0 . To do this, we consider the probabilities of afterpulse events as γ_i , where $P(\gamma_i) = P_0 p_{ap}^i$, and

these events are joint and independent, which means that $P(\gamma_i \cap \gamma_j) = P(\gamma_i)P(\gamma_j) = P_0^2 p_{ap}^{i+j}$.

$$P_{1} = P(\gamma_{0} \cup \gamma_{1}) = P(\gamma_{0}) + P(\gamma_{1}) - P(\gamma_{0} \cap \gamma_{1}) = P_{0}(1 + p_{ap}) - P_{0}^{2}p_{ap},$$

$$P_{2} = P(\gamma_{0} \cup \gamma_{1} \cup \gamma_{2}) = P(\gamma_{0}) + P(\gamma_{1} \cup \gamma_{2}) - P(\gamma_{0} \cap (\gamma_{1} \cup \gamma_{2})) =$$

$$= P(\gamma_{0}) + P(\gamma_{1}) + P(\gamma_{2}) - P(\gamma_{1} \cap \gamma_{2}) - (P(\gamma_{0} \cap \gamma_{1}) + P(\gamma_{0} \cap \gamma_{2}) - P(\gamma_{0} \cap \gamma_{1} \cap \gamma_{2})) =$$

$$= P(\gamma_{0}) + P(\gamma_{1}) + P(\gamma_{2}) - P(\gamma_{0} \cap \gamma_{1}) - P(\gamma_{0} \cap \gamma_{2}) - P(\gamma_{1} \cap \gamma_{2}) + P(\gamma_{0} \cap \gamma_{1} \cap \gamma_{2}) =$$

$$= P_{0}(1 + p_{ap} + p_{ap}^{2}) - P_{0}^{2}(p_{ap} + p_{ap}^{2} + p_{ap}^{3}) + P_{0}^{3}p_{ap}^{3},$$

$$\vdots$$

$$P_{n} = P(\gamma_{0} \cup \gamma_{1} \cup \gamma_{2} \cup \ldots) = P_{0} \sum_{i=0}^{n} p_{ap}^{i} - P_{0}^{2} \sum_{i,j=0;j>i}^{n} p_{ap}^{i+j} + P_{0}^{3} \sum_{i,j,k=0;k>j>i}^{n} p_{ap}^{i+j+k} + \ldots$$

$$(4)$$

In this recursive equation, P_{∞} is the actual probability of the click, which includes all orders of afterpulses. For ease of use in analytical models, we can take the first and second terms in the appropriate order of P_0 . After that, we will analyze the bounds of applicability of these two decomposition models.

We can calculate the sum of the series of first and second order P_0 as follows:

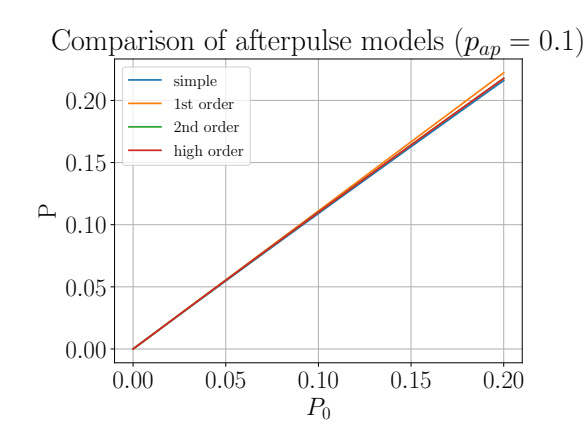
$$\lim_{n \to \infty} \sum_{i=0}^{n} p_{ap}^{i} = \frac{1}{1 - p_{ap}},$$

$$\lim_{n \to \infty} \sum_{i,j=0; j>i}^{n} p_{ap}^{i+j} = \frac{p_{ap}}{(1 - p_{ap})^{2}(1 + p_{ap})}.$$
(5)

So, we can derive the first and second-order afterpulse accounting models as:

1st order:
$$P = P_0 \frac{1}{1 - p_{ap}}$$
,
2nd order: $P = P_0 \frac{1}{1 - p_{ap}} - P_0^2 \frac{p_{ap}}{(1 - p_{ap})^2 (1 + p_{ap})}$. (6)

In figure 2, we compare the detection probability P, calculating according to simple, first, second, and high order models. We assume that high-order model (the decomposition of P with 20th order of P_0) is the benchmark, and we should compare the other models to it. We can see that for low afterpulse probability $p_{ap} = 0.1$ all models give good convergence with the high order model, and the low deviations begin with increasing the P_0 . The first model gives the largest error. However, for the higher values of p_{ap} , we can see that simple and first-order have large deviations. Only a second-order model should be used for accurate estimation of total click probability P.



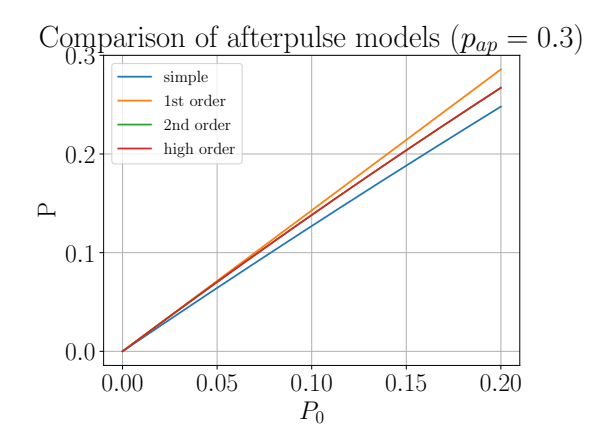


Figure 2: Comparison of the simple, 1st, 2nd and high order models for determining the click probability P, assuming that a) $p_{ap} = 0.1$, b) $p_{ap} = 0.3$.

3 Afterpulse measurement approach

Afterpulse measurements can only be done by processing the triggers histogram, presented in figure 3. In the experimental setup, we set the laser pulse repetition rate equal to 10 kHz and with energy ≈ 1 ph/pulse, i.e., photon arrival time differs by 100 μs . We set the oscilloscope sweep at 25 μs . The photons most likely caused trigger clicks, and these clicks consisted of dark counts and afterpulse counts. After the trigger click bin, we had empty bins during the dead time. In the detector with well-established latched time of the comparator, there was no twilight pulses effect, and during the second dead time, the afterpulse could be described by one of the well-researched laws: exponential [20, 21], power-law [22], and hyberbolic sinc model [23, 24]. Nevertheless, in practice, this is a non-trivial task eliminate twilight pulses, and the first bin after dead time presents this effect - it will be lower than the next bin. In the third and other dead time windows, previous afterpulse clicks' influence distorts the representation of afterpulse law.

As we can see from figure 3 b), the twilight pulse effect is pronounced for low dead time $\tau = 0.21~\mu s$, then for high dead time $\tau = 7.3~\mu s$. The measurement time for these two histograms is equal, and we can see that for high time $t > 10~\mu s$, the count per bin is roughly the same. This figure shows the distribution law of afterpulse and approximates it with one of the three mentioned models.

At the end of the oscilloscope sweep (the range $t_{dcr} \approx [20, 25] \,\mu s$), the count of afterpulse clicks will be negligible, and we can consider that it is mainly due to the dark counts. There is low probability that photon clicks in this time window because of the last's low repetition rate. We will argue that all counts that differ from the dark counts have afterpulse nature

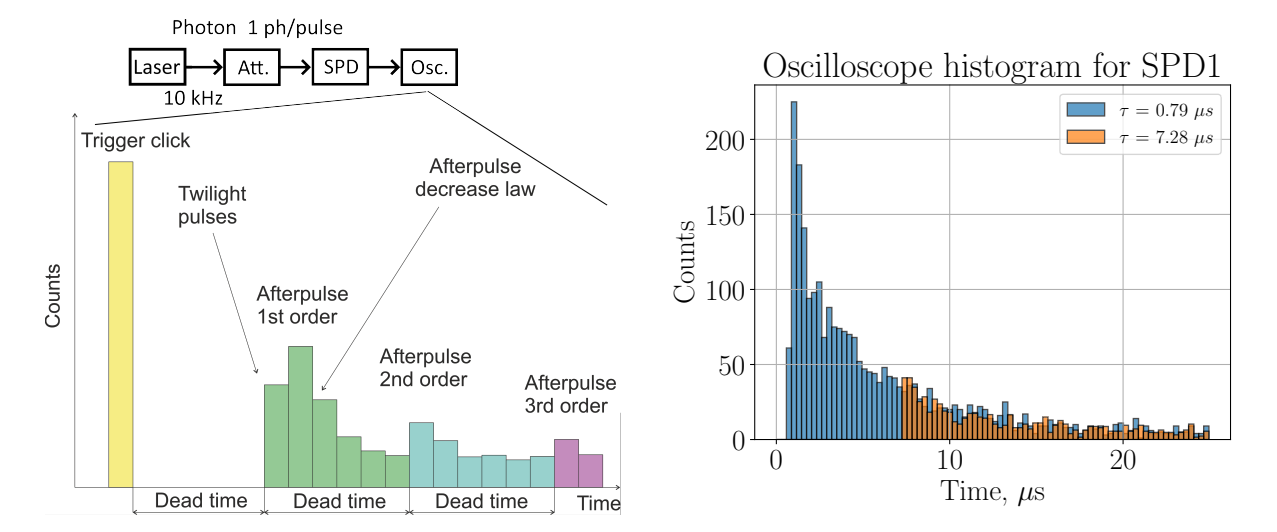


Figure 3: Histogram of the triggers a) schematic form; b) experimental data for SPD1, measured for two different dead times: $\tau = 0.21~\mu s$ and $\tau = 7.3~\mu s$.

for the rough evaluation. Furthermore, the total afterpulse counts can be found as:

$$C_{dcr} = \sum_{i \in t_{dcr}} C_i,$$

$$C_{ap} = \sum_{i \in [0,25]} C_i C_i - C_{dcr},$$

$$(7)$$

where C_{dcr} – is the average DCR counts per bin, C_i – is the count in *i*-th histogram bin, C_{ap} – is the total counts, that we consider as afterpulse counts.

The C_{ap} counts include different orders of afterpulses. We estimate the afterpulse probability as:

$$p_{ap}^{exp} = \frac{C_{ap}}{C_0 - C_{dcr}},\tag{8}$$

where the C_0 – is the counts in trigger zero bin of histogram.

The sense of the estimated value can be described by figure 1 a): $p_{ap}^{exp}P_0 \approx P_{ap} - P_{ap}P_0$. Moreover, we can derive the P_{ap} value that should be universal for all models $P_{ap}^{exp} = p_{ap}^{exp}P_0 = P_{ap}$ as:

$$P_{ap} \approx \frac{p_{ap}^{exp} P_0}{1 - P_0} \tag{9}$$

We can easily calculate the p_{ap} for simple, single, and second-order afterpulse models

with this assumption. We can relate the p_{ap}^{exp} and p_{ap}^{s} and p_{ap} parameters:

$$P_{ap} = \frac{P_n - P_0}{1 - P_0},$$

$$p_{ap}^{exp} P_0 = P_n - P_0,$$

$$P_n = P_0 (1 + p_{ap}^{exp}),$$
(10)

where we obtained the right-hand side for the first equation from the simple equation for P_n (P notation for simple model) probability: $P_n = P_0 + P_{ap} - P_0 P_{ap}$. The P and P_n can be derived from equations 2 and 6 for simple, first and second-order models.

For the simple and first order models, we can get the simple relation for p_{ap}^s and $p_{ap}^{(1)}$:

$$p_{ap}^{s} = \frac{p_{ap}^{exp}}{1 - P_{0}},$$

$$p_{ap}^{(1)} = 1 - \frac{1}{1 + p_{ap}^{exp}}.$$
(11)

Similarly, we can find the $p_{ap}^{(2)}$ for the second-order model, but this is a non-trivial task to do it analytically. For this reason, $p_{ap}^{(2)}$ can be found only numerically.

We can find the $p_{ap}^{(1)}$ value from experimental p_{ap}^{exp} , but to calculate the p_{ap}^s and $p_{ap}^{(2)}$, we need to find the P_0 probability previously. To do this, we need to know the overall probability of click P_n (or P for simple model), which we can find from count rate R and dead time (statistical) τ : $P_n = R\tau$ [25]. After that, we need to paste it into equation 2 or 6 (depends on the observed model) and calculate the P_0 . For the simple model, we can derive the p_{ap}^s value from R analytically:

$$p_{ap}^{s} = \frac{p_{ap}^{exp}(1 + p_{ap}^{exp})}{1 + p_{ap}^{exp} - R\tau}.$$
 (12)

It is evident that with low $R\tau$ the equation 12 takes the following form: $p_{ap}^s = p_{ap}^{exp}$.

For accurate SPD models, one should use the second-order model because $p_{ap}^{(2)}$ does not depend on the P_0 , and one value of $p_{ap}^{(2)}$ can be used for a wide range of optical power per pulse μ (ph/pulse). The simple model is suitable only for low values of p_{ap}^s , and when SPD operation is proposed only with fixed μ . First-order model suits in the case of low $p_{ap}^{(1)}$ because, like for the 2nd order model, it can be used for wide (but lower than for 2nd model) range μ , and simple form of equations allows you to use it in analytical models of SPD.

4 Influence of the active reset on the counting statistics

The principal SPD scheme is presented in figure 4. Here, bias generator apply a DC bias, and sine generator applies the sinusoidal bias to SPAD. Arriving photon can trigger the self-sustaining avalanche process, that leads to high current through SPAD and consequent voltage drop can be registered by comparator and classified as click. After registering the click, comparator is insensitive to new signals during the latching time τ_l (comparator dead time). The quenching process is multistage. The first quenching realized by gated signal – when bias drops below breakdown voltage. Resistor R_q is responsible for passive quenching – it takes up part of the voltage across the diode. But the passive quenching process on the high-frequency (> 100 MHz) sine-gated SPAD may last about hundreds of nanoseconds due to fast voltage relaxation and formation of new avalanche processes. In this quenching regime there are a lot of trapped charges, that sufficiently increase the afterpule probability. This dead time realization we named "Latched time" (LT). In figure 4 this regime corresponds to scheme without quenching driver.

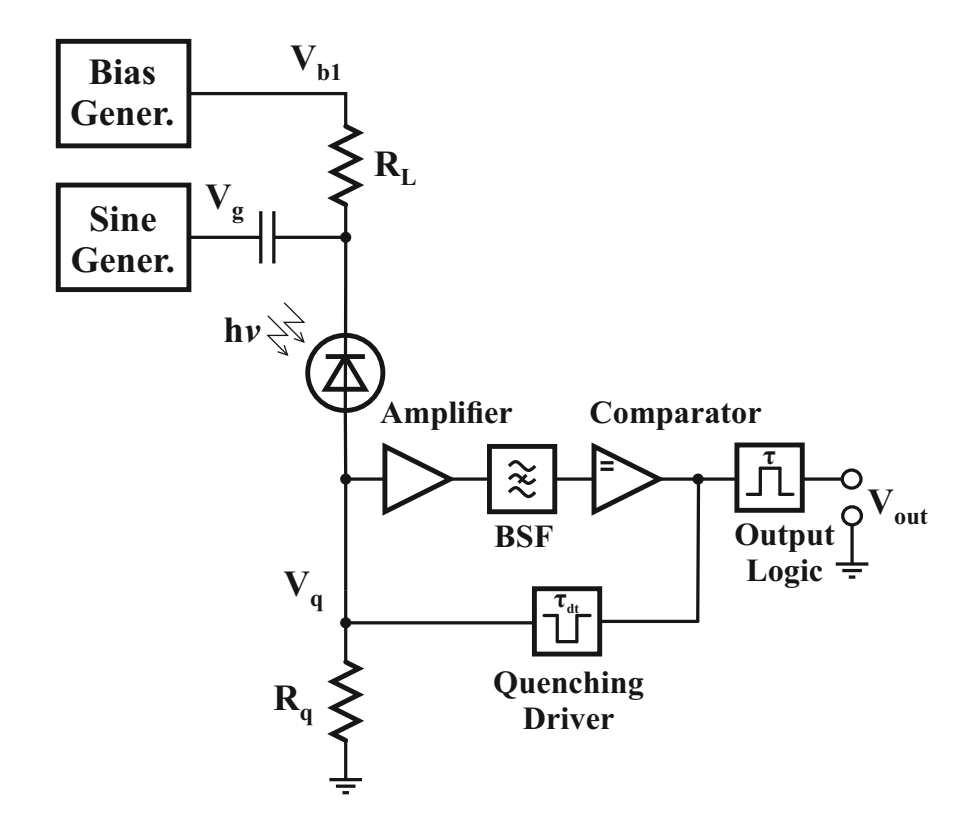


Figure 4: Functional circuit of SPD. In the circuit: Bias Gener. – DC bias generator; Sine Gener. – alternating sinusoidal bias voltage (gate) generator with a frequency of 312.5 MHz; BSF – the barrage filters to eliminate the influence of gates on the processing of avalanche signals.

To avoid problems with many avalanche triggers after the registration event, we need to use active quenching – this is the additional stage in quenching process. We need to note, that this scheme still be the passive quenching, because first quenching is due to passive elements. In figure 4 quenching driver applies the electrical pulse with width τ_c (schematic dead time), that significantly drops the voltage on the SPAD. When SPAD biased under breakdown, it can't be triggered by single photons. The reset to the normal operating regime of the SPAD is due to change of the applying voltage and can be seen as active reset. This dead time realization we named "Latched time + active reset" (LT + AR) [18, 26].

Also, we can define statistical dead time τ_s as the time range between some trigger and the next first possible trigger. This time interval depends on τ_l , τ_c , and active reset pulse form. This pulse should be square in the ideal case, but the leading and trailing edges are distorted due to electronics influence.

Trail edge causes high amplitude oscillations, which are difficult to learn due to their high-frequency components, making detector performance difficult to predict. To exclude possible counting of these triggers, we need to make latched time τ_l more than schematic dead time τ_c on the value, approximately equal to the time of these transients τ_{er} . This recovery time can be in the range $200 < \tau_{er} < 3 \,\mu s$, which depends on the circuit realization, but low values are preferable.

There are different configurations that depend on these time intervals:

- $\tau_l > \tau_c + \tau_{er}$: we present this case in figure 5 a). This figure presents the active reset time and counting statistics for LT and LT + AR schemes (as for the b). Here, latched time fully determines statistical dead time τ_s : $\tau_s = \tau_l$. Here, $\tau_c \approx 3.65 \ \mu s$ and $\tau_{er} \approx 0.8 \ \mu s$. The difference $\tau_l \tau_c \tau_{er} \approx 0.9 \ \mu s$. It means that approximately 0.9 μs in the DT + AR scheme did not detect triggers can occur.
- $\tau_l < \tau_c + \tau_{er}$: we present this case in figure 5 b). Here, $\tau_c \approx 7.5 \ \mu s$, $\tau_{er} \approx 2.5 \ \mu s$, $\tau_l \approx 7.8 \ \mu s$. We can see that the first triggers in the LT + AR scheme occur at 9 μs , which is lower than $\tau_c + \tau_{er} = 10 \ \mu s$. The statistics are due to the SPD's low detection probability when active reset pulse applied to SPAD and its value < 0 because it lowers the bias voltage. The deviation of the initial section of statistics from the mentioned afterpulse laws is determined by the PDE dependence on the SPAD bias voltage. Clicks that occur before full recovery of the bias voltage on the diode are called twilight pulses.

The case, in which using the LT + AR scheme and satisfied $\tau_l \approx \tau_c + \tau_{er}$, where $\tau_{er} \approx 400$ ns is preferable. There are no triggers before the latched time to increase the trap's charge and, consequently, the afterpulse probability. However, setting such a value is a rather non-trivial schematic and technical task.

The next section will compare the LT and LT + AR schemes by the afterpulse probability p_{ap} and show results obtained by simple, first, and second-order models.

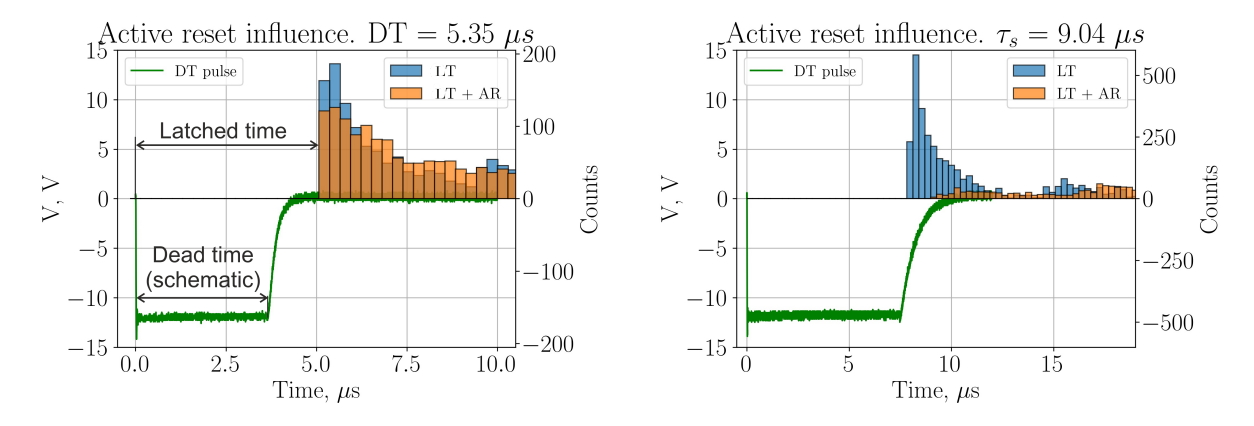


Figure 5: Active reset influence on the counting statistics: a) $\tau_s = 5.35 \ \mu s$; b) $\tau_s = 9.04 \ \mu s$. Two statistics were normalized by zero bin click count $C_0 - C_{dcr}$.

5 Results

3

MF20D300-0001

We tested three custom sinusoidal gated SPDs based on InGaAs/InP SPADs named SPD1, SPD2, and SPD3. These SPADs (with gated frequency $\nu = 312.5$ MHz) were manufactured by Wooriro company and were taken from different batches. The SPAD $N^{\circ}2$ and $N^{\circ}3$ have butterfly housing and a built-in enclosure cooling system. We have shown its main parameters in table 1.

DCR, Hz ($\tau \approx 20 \ \mu s$) SPD $N_{\overline{2}}$ **SPAD** T, K $R = 1200 \; \text{Hz}$ $R = 2200 \; \text{Hz}$ 1 PA19H262-0004 223 ≈ 250 ≈ 450 2 MF20C300-0001 233 ≈ 50 ≈ 100

233

 ≈ 150

 ≈ 300

Table 1: Parameters of used SPADs.

We added the possibility of enabling or disabling quenching driver (passive-active quenching and reset) to the circuit realization of SPD. Also, we added the manual setting of the circuit dead time τ_c and latching time τ_l . In all presented below figures, it was $\tau_l > \tau_c$. However, due to transients at the trailing edge during the τ_{er} , we cannot accurately set the parameters to achieve the preferable condition: $\tau_l > \tau_c + \tau_{er}$. For this reason, some data was obtained for the first case and another for the second case of time interval configurations, presented above. It means that statistical dead time τ_s for LT and LT + AR schemes can differ for the similar setting of latched time.

In our experiments, laser pulses with FWHM ≈ 50 ps and repetition rate 10 kHz were attenuated to the average power per pulse $\mu \approx 1$ ph/pulse. We established two count rates

in our experiments: $R \approx 1200$ Hz and $R \approx 2200$ Hz. It means that for low p_{ap} values $(p_{ap} < 5\%)$ $PDE \approx 10\%$ and $PDE \approx 20\%$ correspondingly. Nevertheless, for the high p_{ap} values, PDE was lowered. The setting of the R value was performed by changing the SPD's bias voltage with unchanged gate amplitude. The statistics was collected on an oscilloscope and processed to obtain p_{ap}^{exp} value. After that, we found p_{ap}^{s} , $p_{ap}^{(1)}$ and $p_{ap}^{(2)}$, which correspond to simple, first, and second-order models.

In figure 6 a), we present the p_{ap} value for LT and LT + AR schemes obtained for simple and second-order models (diamond and point markers correspondingly). We approximated data for SPD1 and SPD2 curves defined by the power-law equation. Data for SPD3 was approximated with an exponential equation:

power law:
$$p_{ap}^{pl}(\tau) = A\tau^B + C$$
,
exponential: $p_{ap}^e(\tau) = Ae^{-B\tau} + C$, (13)

where the A, B and C parameters presented in the table 2 from appendix A.

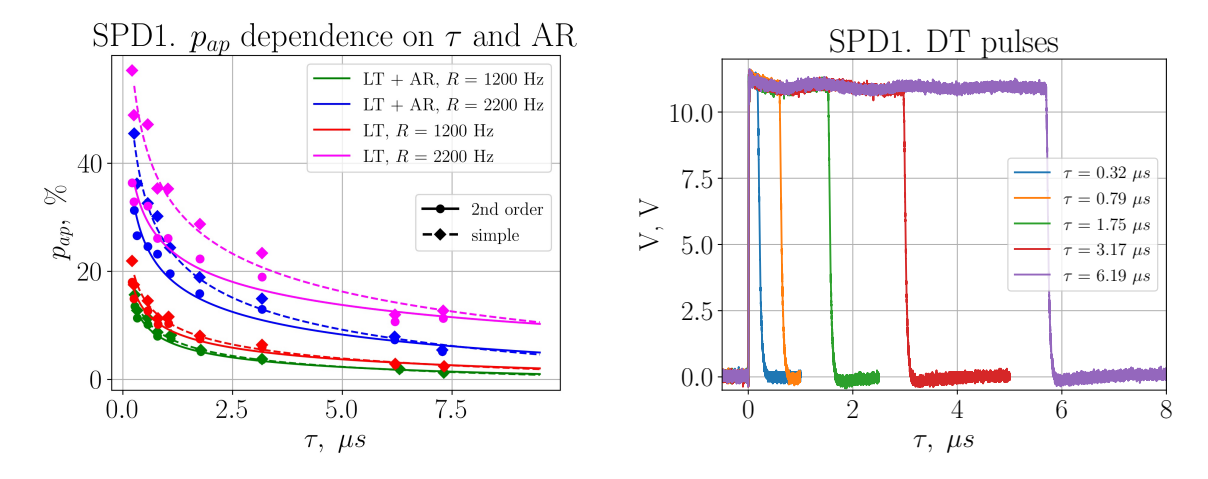


Figure 6: SPD1 data: a) Comparing p_{ap} for LT and LT + AR schemes, obtained in according to simple and second-order models (diamonds and points correspondingly). Dashed lines represent the fitted curves for simple model, solid lines – for the second-order model; b) Active reset pulse, applied to SPAD after the trigger.

The common used law for approximate the p_{ap} dependence on the dead time for fixed PDE is the exponential, as shown in works [16–19,27–29]. But in our work we fixed the total counts R, that can be considered as fixed PDE only for low p_{ap} (the SPD3 has low p_{ap} and data had been approximated with exponential law quite well). We didn't fix the PDE value instead because there is not consensus for it's definition equation. On countrary, experimentally obtained counting rates can be defined only one way.

In this figure, we can see that afterpulse probability estimation p_{ap} at the high values and low τ values sufficiently differs for simple and second-order models – solid and dashed

curves. However, for low p_{ap} and high τ they almost coincide. We can see that using active reset has significant effects on the pap, which is especially noticeable for R = 2200 Hz. We can also see that with higher bias voltage on SPAD, which is directly related to R, the afterpulse probability is high.

Figure 6 b) presents the active reset pulses. The leading edge is sharp in order to remove possible triggers that may occur quickly. In this case, high-amplitude transient processes occur, but they do not influence triggers. The trailing edge is smoother to reduce the internal transients' time interval and make its amplitude lower.

Figure 7 is similar to figure 6 but performed for SPD2. We can see that for R = 2200 Hz, p_{ap} is sufficiently higher than p_{ap} for SPD1, and vice versa for R = 1200 Hz. This feature is not due to the control circuit but due to differences in the SPAD's characteristics. In figure b), we can see that the trailing edge is sufficiently smoother. For SPD1, that can cause intense twilight pulses and reduce SPAD efficiency for high-frequency laser pulse repetition rates.

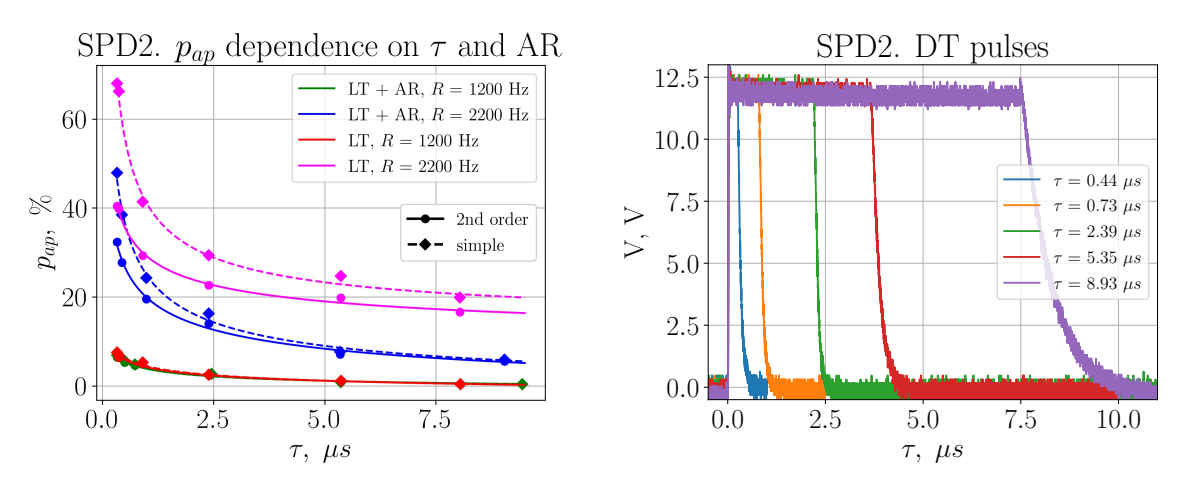
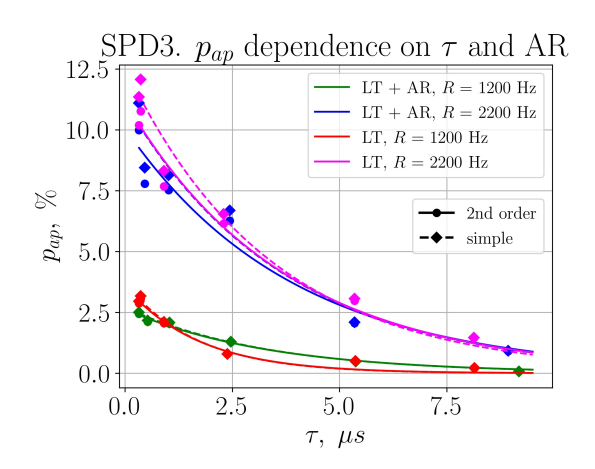


Figure 7: SPD2 data: a) Comparing p_{ap} for LT and LT + AR schemes, obtained in according to simple and second-order models (diamonds and points correspondingly). Dashed lines represent the fitted curves for simple model, solid lines – for the second-order model; b) Active reset pulse, applied to SPAD after the trigger.

Figure 8 a) presents the same, as in figures 6 and 7, but for SPD3 data. The afterpulse probability for this detector is small enough even for low dead time and disabled active reset. For the $R=1200~{\rm Hz}$ data, the LT red curve lies lower than LT + AR green curve. Here it is already a matter of measurement errors and the features of the approximation of experimental data.

Figure 8 b) compares the p_{ap}^s , $p_{ap}^{(1)}$ and $p_{ap}^{(2)}$ with p_{ap}^{exp} for the SPD2 data and R=2200 Hz. We can see that the first and second-order models have a satisfactory agreement for high afterpulse probabilities and sufficiently differ from experimentally obtained p_{ap}^{exp} . These models differ for the afterpulse probability $p_{ap}^{exp} < 15$ %. The simple model for a high $p_{ap}^{exp} > 15$ % tends to this p_{ap}^{exp} value. However, for a lower p_{ap}^{exp} , it has even more value.



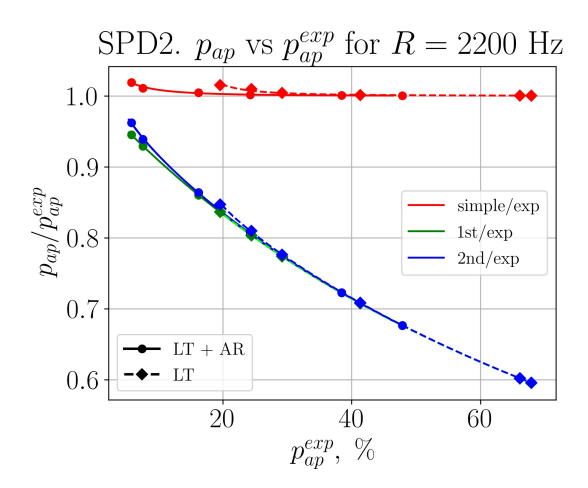


Figure 8: a) SPD3 data: comparing of p_{ap} for LT and LT + AR schemes, obtained in according to simple and second-order models (diamonds and points correspondingly). Dashed lines represent the fitted curves for simple model, solid lines – for the second-order model; b) SPD2 data: comparing of p_{ap}^s , $p_{ap}^{(1)}$ and $p_{ap}^{(2)}$ with p_{ap}^{exp} for the SPD2 data and R = 2200 Hz.

There is no sufficient difference between the LT or LT + AR schemes – they converge quite well on these graphs.

We can make the main conclusions of this schedule:

- There is no difference in p_{ap} for the LT and LT + AR schemes for high τ values and low R (related with PDE) rates. If SPD is not designed with strict requirements for limiting count rates and quantum efficiency, then it is permissible not to use a circuit with active reset pulses.
- Choosing a model for calculating the p_{ap} is essential for high afterpulse probabilities $(p_{ap}^{exp} > 5 \%)$ first, or second-order models are preferable. For low values p_{ap}^{exp} , we can use a simple model too. According to the simple model, we get a strongly overestimated value of the afterpulse, which coincides with the experimentally found one.

6 Conclusion

The main result of the work is that we compare schemes with latching time (LT) and with latching time and active reset (LT + AR) and its influence on the afterpulse probability. As a result of the experiments, we have shown that an active reset module could significantly reduce afterpulse probability. However, with large dead time ($\tau > 10~\mu s$) and generally low afterpulse probabilities ($p_{ap}^{exp} < 5~\%$), the differences between the two schemes are relatively insignificant. With low requirements for the detector ($\tau > 5~\mu s$ and PDE =

10 %), the possibility of abandoning the active reset module will significantly simplify the detector's circuit design. At the same time, insignificantly increase the afterpulse probability. We need to mention, that we performed all our measurements on the 10 kHz laser pulses repetition rate. For high laser pulse repetition rates (> 1 MHz), in the LT scheme afterpulse probability will sufficiently increase due to generating additional avalanche processes during the latching time.

The second result is the developed approach to determining the probability of afterpulses of detectors, following three models. We have described the procedure for processing statistics from the oscilloscope histograms to obtain the experimental afterpulse probability. We introduce three models: simple, 1-st and 2-nd order. We obtain, that simple model is not appropriate for description of the afterpulsing counting statistics due to rough underlied physical processes. As a result of the experiments, it was shown that the use of the simple model gives rough results, which at high afterpulse probabilities tend to simplify experimentally obtained values. We have shown that it is best to use the second-order model, which should give correct results for both small and large afterpulse probabilities. If the use of the analytical applications model is required, then the first-order model should be used because of its simple algebraic form. Obtained with this model results have small deviations from the second-order model with the afterpulse probability $p_{ap}^{exp} < 15$ %, but for large values, they coincide well.

Other work results are the given recommendations for setting the values of the circuit dead time and latching time from the conditions of the internal transient time. Also, tables with fitted parameters were presented, approximating the results obtained for a simple model and a second-order model, which allows using these dependencies in the global SPD model.

A Table with fitted parameters

For the simple and second order models we present the parameters of fitted curves in the table 2:

Table 2: Parameters of the fitted curves for simple and second order models.

SPD№	Fit equation	Scheme	R, Hz	Model	A	В	С
SPD1	Power law	LT	1200	simple	0.004	-0.276	-0.084
				2nd order	0.004	-0.27	-0.068
			2200	simple	0.041	-0.2	-0.31
				2nd order	0.036	-0.18	-0.185
		LT + AR	1200	simple	0.001	-0.34	-0.053
				2nd order	0.001	-0.346	-0.043
			2200	simple	0.011	-0.266	-0.201
				2nd order	0.013	-0.238	-0.152
SPD2	Power law	LT	1200	simple	0.0026	-0.26	-0.05
				2nd order	0.003	-0.25	-0.05
			2200	simple	6e-5	-0.615	0.128
				2nd order	0.001	-0.373	0.067
		LT + AR	1200	simple	2e-4	-0.397	-0.019
				2nd order	0.001	-0.292	-0.03
			2200	simple	3e-4	-0.509	0.035
				2nd order	0.004	-0.308	-0.095
SPD3	Exponential	LT	1200	simple	0.036	7.7e5	0.003
				2nd order	0.034	7.6e5	0.003
			2200	simple	0.115	4.1e5	0.015
				2nd order	0.103	3.3e5	0.0098
		LT + AR	1200	simple	0.029	2.6e5	-0.002
				2nd order	0.029	2e5	-0.004
			2200	simple	0.116	2.5e5	-0.005
				2nd order	0.107	2.2e5	-0.008

References

- [1] L. You, "Superconducting nanowire single-photon detectors for quantum information," *Nanophotonics*, vol. 9, no. 9, pp. 2673–2692, 2020.
- [2] C. Bruschini, H. Homulle, and E. Charbon, "Ten years of biophotonics single-photon spad imager applications: retrospective and outlook," in *Multiphoton Microscopy in the Biomedical Sciences XVII*, vol. 10069. International Society for Optics and Photonics, 2017, p. 100691S.
- [3] J. Chang, J. Los, J. Tenorio-Pearl, N. Noordzij, R. Gourgues, A. Guardiani, J. Zichi, S. Pereira, H. Urbach, V. Zwiller *et al.*, "Detecting telecom single photons with 99.5-2.07+ 0.5% system detection efficiency and high time resolution," *APL Photonics*, vol. 6, no. 3, p. 036114, 2021.
- [4] C. Agnesi, M. Avesani, L. Calderaro, A. Stanco, G. Foletto, M. Zahidy, A. Scriminich, F. Vedovato, G. Vallone, and P. Villoresi, "Simple quantum key distribution with qubit-based synchronization and a self-compensating polarization encoder," *Optica*, vol. 7, no. 4, pp. 284–290, 2020.
- [5] Z. Zhang, C. Chen, Q. Zhuang, F. N. Wong, and J. H. Shapiro, "Experimental quantum key distribution at 1.3 gigabit-per-second secret-key rate over a 10 db loss channel," *Quantum Science and Technology*, vol. 3, no. 2, p. 025007, 2018.
- [6] J.-P. Chen, C. Zhang, Y. Liu, C. Jiang, W. Zhang, X.-L. Hu, J.-Y. Guan, Z.-W. Yu, H. Xu, J. Lin et al., "Sending-or-not-sending with independent lasers: Secure twin-field quantum key distribution over 509 km," Physical review letters, vol. 124, no. 7, p. 070501, 2020.
- [7] E. O. Kiktenko, N. O. Pozhar, A. V. Duplinskiy, A. A. Kanapin, A. S. Sokolov, S. S. Vorobey, A. V. Miller, V. E. Ustimchik, M. N. Anufriev, A. Trushechkin et al., "Demonstration of a quantum key distribution network in urban fibre-optic communication lines," Quantum Electronics, vol. 47, no. 9, p. 798, 2017.
- [8] L.-Y. Zhao, Q.-J. Wu, H.-K. Qiu, J.-L. Qian, and Z.-F. Han, "Practical security of wavelength-multiplexed decoy-state quantum key distribution," *Physical Review A*, vol. 103, no. 2, p. 022429, 2021.
- [9] C. Wang, J. Wang, Z. Xu, J. Li, R. Wang, J. Zhao, and Y. Wei, "Afterpulsing effects in spad-based photon-counting communication system," *Optics Communications*, vol. 443, pp. 202–210, 2019.
- [10] H. Wang, H. Li, L. You, Y. Wang, L. Zhang, X. Yang, W. Zhang, Z. Wang, and X. Xie, "Fast and high efficiency superconducting nanowire single-photon detector at 630 nm wavelength," *Applied optics*, vol. 58, no. 8, pp. 1868–1872, 2019.

- [11] S. C. Wein, J.-W. Ji, Y.-F. Wu, F. K. Asadi, R. Ghobadi, and C. Simon, "Analyzing photon-count heralded entanglement generation between solid-state spin qubits by decomposing the master-equation dynamics," *Physical Review A*, vol. 102, no. 3, p. 033701, 2020.
- [12] E. Sarbazi, M. Safari, and H. Haas, "The impact of long dead time on the photo-count distribution of spad receivers," in 2018 IEEE Global Communications Conference (GLOBECOM). IEEE, 2018, pp. 1–6.
- [13] M. A. Smirnov, N. S. Perminov, R. R. Nigmatullin, A. A. Talipov, and S. A. Moiseev, "Sequences of the ranged amplitudes as a universal method for fast noninvasive characterization of spad dark counts," *Applied optics*, vol. 57, no. 1, pp. 57–61, 2018.
- [14] D. Kramnik and R. J. Ram, "Efficient statistical separation of primary dark counts and afterpulses in free-running spads," in *CLEO: Applications and Technology*. Optical Society of America, 2020, pp. JTh2A–29.
- [15] G.-J. Fan-Yuan, J. Teng, S. Wang, Z.-Q. Yin, W. Chen, D.-Y. He, G.-C. Guo, and Z.-F. Han, "Optimizing single-photon avalanche photodiodes for dynamic quantum key distribution networks," *Physical Review Applied*, vol. 13, no. 5, p. 054027, 2020.
- [16] J. C. Campbell, W. Sun, Z. Lu, M. A. Itzler, and X. Jiang, "Common-mode cancellation in sinusoidal gating with balanced ingaas/inp single photon avalanche diodes," *IEEE Journal of Quantum Electronics*, vol. 48, no. 12, pp. 1505–1511, 2012.
- [17] J. Liu, Y. Li, L. Ding, Y. Wang, T. Zhang, Q. Wang, and J. Fang, "Fast active-quenching circuit for free-running ingaas (p)/inp single-photon avalanche diodes," *IEEE Journal of Quantum Electronics*, vol. 52, no. 10, pp. 1–6, 2016.
- [18] J. Liu, Y. Xu, Y. Li, Y. Gu, Z. Liu, and X. Zhao, "Ultra-low dead time free-running ingasp single-photon detector with active quenching," *Journal of Modern Optics*, vol. 67, no. 13, pp. 1184–1189, 2020.
- [19] Y.-Q. Fang, W. Chen, T.-H. Ao, C. Liu, L. Wang, X.-J. Gao, J. Zhang, and J.-W. Pan, "Ingaas/inp single-photon detectors with 60% detection efficiency at 1550 nm," *Review of Scientific Instruments*, vol. 91, no. 8, p. 083102, 2020.
- [20] B. Korzh, T. Lunghi, K. Kuzmenko, G. Boso, and H. Zbinden, "Afterpulsing studies of low-noise ingaas/inp single-photon negative-feedback avalanche diodes," *Journal of Modern Optics*, vol. 62, no. 14, pp. 1151–1157, 2015.
- [21] G. Humer, M. Peev, C. Schaeff, S. Ramelow, M. Stipčević, and R. Ursin, "A simple and robust method for estimating afterpulsing in single photon detectors," *Journal of Lightwave Technology*, vol. 33, no. 14, pp. 3098–3107, 2015.

- [22] M. A. Itzler, X. Jiang, and M. Entwistle, "Power law temporal dependence of ingaas/inp spad afterpulsing," *Journal of Modern Optics*, vol. 59, no. 17, pp. 1472–1480, 2012.
- [23] D. Horoshko, V. Chizhevsky, and S. Y. Kilin, "Afterpulsing model based on the quasicontinuous distribution of deep levels in single-photon avalanche diodes," *Journal of Modern Optics*, vol. 64, no. 2, pp. 191–195, 2017.
- [24] A. W. Ziarkash, S. K. Joshi, M. Stipčević, and R. Ursin, "Comparative study of afterpulsing behavior and models in single photon counting avalanche photo diode detectors," *Scientific reports*, vol. 8, no. 1, pp. 1–8, 2018.
- [25] A. Koziy, A. Tayduganov, A. Losev, V. Zavodilenko, A. Gorbatsevich, and Y. Kurochkin, "Investigating the coherent state detection probability of ingaas/inp spad-based single-photon detectors," 2021.
- [26] J. Liu, Y. Xu, Y. Li, Z. Liu, and X. Zhao, "Exploiting the single-photon detection performance of ingaas negative-feedback avalanche diode with fast active quenching," *Optics Express*, vol. 29, no. 7, pp. 10150–10161, 2021.
- [27] A. Tosi, N. Calandri, M. Sanzaro, and F. Acerbi, "Low-noise, low-jitter, high detection efficiency ingaas/inp single-photon avalanche diode," *IEEE Journal of selected topics* in quantum electronics, vol. 20, no. 6, pp. 192–197, 2014.
- [28] J. Liu, T. Zhang, Y. Li, L. Ding, J. Tao, Y. Wang, Q. Wang, and J. Fang, "Design and characterization of free-running ingaasp single-photon detector with active-quenching technique," *Journal of Applied Physics*, vol. 122, no. 1, p. 013104, 2017.
- [29] J. Kirdoda, D. C. Dumas, R. W. Millar, M. M. Mirza, D. J. Paul, K. Kuzmenko, P. Vines, Z. Greener, and G. S. Buller, "Geiger mode ge-on-si single-photon avalanche diode detectors," in 2019 IEEE 2nd British and Irish Conference on Optics and Photonics (BICOP). IEEE, 2019, pp. 1–4.